PARALLEL CONSTRUCTION OF NONLINEAR FORCE-FREE FIELDS

M. S. WHEATLAND
School of Physics, University of Sydney, NSW 2006, Australia
(e-mail: m.wheatland@physics.usyd.edu.au)

(Received 29 February 2004; accepted 5 May 2004)

Abstract. A numerical approach to calculating nonlinear force-free fields is presented. The approach is similar to Sakurai (1981) being a current-field iteration scheme using the integral solution to Ampere's law (the Biot–Savart law). However, the method of solution presented here is simpler than Sakurai's approach, in that the field is directly constructed on a grid without the intermediate solution of a large system of nonlinear equations. The method also permits straightforward implementation on parallel computers. Results of applying the method to a number test cases, including boundary conditions with substantial currents, are presented.

1. Introduction

Solar coronal magnetic fields are the source of energy for solar flares (e.g., Priest and Forbes, 2002), and play an important but incompletely understood role in coronal heating. Direct measurement of the field in the corona is difficult (however, see Lin, Penn, and Tomczyk, 2000), and the most detailed information comes from the influence of the field on magnetically sensitive lines at the photosphere and in the chromosphere. There is considerable interest in techniques for reconstructing the field in the corona based on these measurements. Accurate coronal field reconstructions are even more important with the advent of a new generation of ground- and space-based vector magnetographs, in particular SOLIS (Keller, Harvey, and Giampapa, 2003), and the proposed *Solar Dynamics Observatory* and *Solar*-B instruments.

A popular model for the magnetic field $\mathbf{B}$ in the solar corona is that it is force-free, i.e., the field is assumed to satisfy the force-free equation

$$(\nabla \times \mathbf{B}) \times \mathbf{B} = 0, \tag{1}$$

as well as $\nabla \cdot \mathbf{B} = 0$. Physically the force-free state corresponds to a static situation in which the magnetic (Lorentz) force dominates over plasma forces. The force-free Equation (1) may also be written

$$\nabla \times \mathbf{B} = \alpha \mathbf{B}, \tag{2}$$

where α is in general a function of position. Taking the divergence of this equation gives the prescription

Solar Physics **222:** 247–264, 2004.

$$\mathbf{B} \cdot \nabla \alpha = 0 \tag{3}$$

which means that α is a constant along a field line.

The simplest force-free models are the potential field model ($\alpha = 0$) and the linear force-free model ($\alpha =$ constant). In these cases there are integral solutions for the field in a volume in terms of the normal component of the field on the boundary of the volume and the value of α, although in the linear case the solution is not unique (e.g., Alissandrakis, 1981). These solutions are still widely used in solar physics to model coronal fields, both for simple test cases, and using vector magnetograph boundary data. However, the potential and linear force-free models have serious deficiencies. For example, potential fields have no free energy, and linear force-free fields generally have infinite energy in a half space.

Nonlinear force-free fields correspond to spatially varying α. In this case analytic solutions are only available for limited cases with specific symmetries (e.g., Marsh, 1996). The appropriate boundary conditions for existence and uniqueness of a solution are not rigorously proven, although it is often argued that the normal component of the field on the boundary together with the distribution of α over one of the magnetic polarities is sufficient to determine a solution, provided all field lines connect to the boundary (Grad and Rubin, 1958). Bineau (1972) demonstrated that these boundary conditions ensure a unique solution for small values of α.

A variety of approximate numerical methods have been proposed for calculating nonlinear force-free fields (for reviews see e.g., Sakurai, 1989; McClymont, Jiao, and Mikić, 1997; Amari *et al.*, 1997; for recent developments see, e.g., Wheatland, Sturrock, and Roumeliotis, 2000; Yan and Sakurai, 2000; Li, Wang, and Wei, 2003; Wiegelmann and Inhester, 2003). All methods are computationally intensive, and it is fair to say that to date they are not routinely applied in solar physics.

One mathematically well-founded approach is current-field iteration (Grad and Rubin, 1958), which can be summarized as the solution, at iteration $k + 1$, of the linear equations

$$\nabla \times \mathbf{B}^{k+1} = \alpha^k \mathbf{B}^k \tag{4}$$

and

$$(\mathbf{B}^{k+1} \cdot \nabla)\alpha^{k+1} = 0. \tag{5}$$

Equation (4) is an updating of the field at iteration $k + 1$ based on the current distribution at iteration k. Equation (5) is a propagation of α^{k+1} along the updated field lines, i.e., an updating of the current distribution. The proofs of existence and uniqueness by Bineau (1972) are based on current-field iteration.

Sakurai (1981) presented a numerical scheme for implementing current-field iteration. In this approach a number of field lines of an initial potential field are traced, and the integral solution to Equation (4)

$$\mathbf{B}(\mathbf{x}) = \frac{\mu_0}{4\pi} \int \mathrm{d}V' \mathbf{J}(\mathbf{x}') \times \frac{\mathbf{x} - \mathbf{x}'}{|\mathbf{x} - \mathbf{x}'|^3} \tag{6}$$

(the Biot–Savart law), is used to calculate a perturbation to the potential field due to currents added along the chosen field lines. To make the iteration procedure computationally feasible, Sakurai adopted a set of nodal points along the chosen field lines as the free parameters in the problem. A pair of nodal points defines the axis of a current element. Requiring that the net field due to the Biot–Savart contributions from all current elements is parallel to the axis at the centre of each current element leads to a set of coupled nonlinear equations for the locations of the nodal points. These equations were solved using the iterative quasi-Newton method. The initial results produced by Sakurai were promising, but the method does not appear to have been subsequently developed. McClymont, Jiao, and Mikić (1997) state that the method does not converge for highly non-potential fields, and Amari *et al.* (1997) suggest that this is related to the sensitive convergence properties of the system of nonlinear equations.

Recently a different approach to current-field iteration has been formulated (Amari *et al.*, 1997; Amari, Boulmezaoud, and Mikić, 1999). In this case the vector potential is used and the analog of Equation (4) is solved by discretization and solution of a linear system of equations. This method has been shown to successfully reconstruct a test solution (Amari, Boulmezaoud, and Mikić, 1999), and has also been applied to vector magnetograph data (Régnier, Amari, and Kersalé, 2002). Amari *et al.* (1997) state that the vector potential is used to ensure that the divergence of the field is zero. However, we note that the approach of Sakurai (1981) also ensures this, since the divergence of Equation (6) is zero.

In this paper another implementation of current-field iteration is described, which is closest to Sakurai's method. However, the present method is simpler to implement than the methods of Sakurai (1981) or Amari, Boulmezaoud, and Mikić (1999) in that it does not involve the solution of a large system of nonlinear or linear equations respectively – at each iteration the field is directly constructed on a grid. A feature of the method is that it is straightforward to implement for parallel computation. This is an important consideration because: (1) force-free reconstructions are computationally intensive, in particular when applied to modern high-resolution vector magnetograph data; and (2) parallel computers, in particular distributed memory clusters are now widely available to solar researchers. A brief description of the code and of preliminary results was given in Wheatland (2004). This paper presents a more detailed account.

The layout of this paper is as follows. In Section 2 the computational method is described. In Section 3 the results of applying the method to simple test cases are presented, and in Section 4 the results are discussed.

2. Method

2.1. Description

The method is implemented on a cartesian grid [a gridpoint is here denoted $\mathbf{x} = (x, y, z)$], with the lower boundary ($z = 0$) representing the photosphere. Uniform and equal grid spacings $\Delta x = \Delta y = \Delta z$ are assumed, with N gridpoints along each dimension.

An initial potential field $\mathbf{B}_0(\mathbf{x})$ is calculated for every gridpoint $\mathbf{x}$ based on given boundary values $B_z(x, y, 0)$. The other boundary values imposed are a set of values α_i ($i = 1, 2, \ldots, M$) of the force-free parameter at M lower boundary gridpoints with positive polarity [a chosen set of points $(x_i, y_i, 0)$ such that $B_z(x_i, y_i, 0) > 0$]. These points are taken to be the footpoints for current-carrying field lines.

The field line of the potential field starting from the position $(x_i, y_i, 0)$ of footpoint i is traced, using fourth order Runge–Kutta and linear interpolation of $\mathbf{B}_0(\mathbf{x})$ between gridpoints. Following Sakurai (1981), field line i is modelled as current-carrying by assuming a sequence of short cylindrically symmetric current elements between nodal points along the field line. It is also assumed that there is a mirror image current-carrying field line in $z < 0$, so that a complete circuit of current passes through footpoint i. A contribution $\Delta\mathbf{B}_{1,i}(\mathbf{x})$ to the field due to the current circuit i is calculated at all gridpoints $\mathbf{x}$ using the Biot-Savart law (Equation (6)), as follows. This field contribution is the sum $\Delta\mathbf{B}_{1,i}(\mathbf{x}) = \sum_j \Delta\mathbf{B}_{1,i,j}(\mathbf{x})$ over contributions from each current element in the circuit (the current elements for the given field line i are enumerated by j). For gridpoints far from the centre of current element j, the asymptotic form

$$\Delta\mathbf{B}_{1,i,j}(\mathbf{x}) = \frac{\mu_0}{4\pi} I_i \mathbf{l}_j \frac{\mathbf{x} - \mathbf{x}'_j}{|\mathbf{x} - \mathbf{x}'_j|^3} \tag{7}$$

of the Biot–Savart law is used, where $\mathbf{l}_j$ is the vector joining the nodal points defining the axis of current element j, $\mathbf{x}'_j$ is the centre of the current element, and I_i is the total current along the field line. For gridpoints closer to $\mathbf{x}'_j$ the approach of Sakurai (1981) is followed: the current density is assumed to follow a Gaussian distribution $J_j(r_j) = J_{0,j} e^{-r_j^2/a_j^2}$ [where $J_{0,j} \equiv I_i/(\pi a_j^2)$] with respect the axis of the current element, in which case the exact counterpart of Equation (6) is

$$\Delta B_{\phi\,1,i,j}(\mathbf{x}) = \frac{\mu_0 I_i}{2\pi} \int_0^\infty \mathrm{d}k J_1(kr_j) e^{-a_j^2 k^2/4} \times \times \begin{cases} e^{-k|z_j|} \sinh(kl_j/2) & (|z_j| > l_j/2) \\ 1 - e^{-kl_j/2} \cosh(kz_j) & (|z_j| < l_j/2), \end{cases} \tag{8}$$

where r_j, ϕ_j, z_j are local cylindrical coordinates defined by the origin $\mathbf{x}'_j$ and the axis $\mathbf{l}_j$. In practice we find that Equation (7) is accurate to a few percent provided $|\mathbf{x} - \mathbf{x}'_j| > f \times \max(a_j, l_j)$, where $f \approx 5$. This means that the simple expression (7)

can be used for the great majority of gridpoints, and the integral (8) need only be evaluated for a relatively small fraction of gridpoints. The integral is evaluated using the trapezoidal rule. Finally it should be noted that, again following Sakurai, the radius a_j of the current elements is assumed to expand with neighboring field lines. At the footpoint of the field line the radius $a_0 = (\Delta x \Delta y/\pi)^{1/2}$ is adopted. The current along the field line is then $I_i = \pi a_0^2 \alpha_i B_{z,0}/\mu_0$, where $B_{z,0,i} = B_z(x_i, y_i, 0)$ is the vertical component of field at the footpoint. For current element j the radius is taken to be $a_j = (B_{z,0,i}/B_{\parallel,j})^{1/2} a_0$, where $B_{\parallel,j}$ is the magnitude of the component of field along the axis of the current element. This choice implies that the radius of the current element expands with the field whilst conserving current.

The procedure described in the previous paragraph is repeated for all M field lines, to produce a net contribution $\Delta\mathbf{B}_1(\mathbf{x}) = \sum_i \Delta\mathbf{B}_{1,i}(\mathbf{x})$ at every gridpoint $\mathbf{x}$ in the box. Then the procedure is iterated. Fieldlines of the perturbed field $\mathbf{B}_1(\mathbf{x}) = \mathbf{B}_0(\mathbf{x}) + \Delta\mathbf{B}_1(\mathbf{x})$ are traced starting from each footpoint $(x_i, y_i, 0)$, and contributions $\Delta\mathbf{B}_2(\mathbf{x})$ due to current along these field lines are calculated, leading to a net field $\mathbf{B}_2(\mathbf{x}) = \mathbf{B}_0(\mathbf{x}) + \Delta\mathbf{B}_2(\mathbf{x})$. This procedure is repeated for K iterations, leading to an estimate $\mathbf{B}_K(\mathbf{x})$ for a force-free field, calculated at every gridpoint.

Before proceeding we highlight the distinction between the present method and Sakurai (1981). In Sakurai's approach nodal points along field lines are introduced as the free parameters in the problem. This is presumably to avoid direct construction of the field at every gridpoint, which would involve evaluation of integrals (Equation (8)) over every current element for every gridpoint. In the present method the field is directly constructed, but the procedure is made computationally feasible by introducing the asymptotic form (7), which greatly reduces the number of integrals to be evaluated.

2.2. PARALLELIZATION

A feature of the present method is that the contributions $\Delta\mathbf{B}_{k,i}(\mathbf{x})$ at iteration k may be calculated independently for each of the M current-carrying field lines. The physical basis for this is the trivial point that Ampere's law is linear. This provides a natural way to parallelize the method. The independent calculations need to be synchronized when the sum $\Delta\mathbf{B}_k(\mathbf{x}) = \sum_i \Delta\mathbf{B}_{k,i}(\mathbf{x})$ is evaluated. This is a common problem in parallel computing called sum reduction (e.g., Chandra *et al.*, 2001), which is straightforward to implement.

In the simplest implementation, each independent process or thread of the code has a copy of the three-dimensional array $\mathbf{B}_k(\mathbf{x})$, which is used to trace field line i. Each process then calculates its own three-dimensional array $\Delta\mathbf{B}_{k,i}(\mathbf{x})$, based on its field line. A master process synchronizes the addition of the $\Delta\mathbf{B}_{k,i}(\mathbf{x})$. In practice each process is given a subset of the M field lines, rather than just one field line, and calculates the contribution due to field lines in that subset.

The method of parallelization is described in detail because it is different from usual approaches. Typically codes are parallelized by decomposing the computa-

tional grid, and having each process operate on a section of the grid. The present method is simpler than such an approach and requires less inter-process communication. A disadvantage of the present approach is that each process must deal with arrays as large as the total array, so sufficient memory must be available to each process. The method of parallelization is discussed in more detail in Section 4.

3. Results

The method has been initially tested by application to a number of test cases, including configurations similar to those presented by Sakurai (1981). The code used is a parallel implementation using OpenMP (Chandra *et al.*, 2001) run on an eight-processor shared memory machine. The tests involve a grid with $N = 100$, and a moderate number of current-carrying field lines (54).

For each test case the boundary condition on the normal component of **B** is chosen to be the simple bipolar configuration:

$$\begin{aligned} B_z(x, y, 0) = \; & B_0 \exp\left[-\frac{(x - x_{1+})^2}{2\sigma^2} - \frac{(y - y_{1+})^2}{2\sigma^2}\right] - \\ & -B_0 \exp\left[-\frac{(x - x_{1-})^2}{2\sigma^2} - \frac{(y - y_{1-})^2}{2\sigma^2}\right], \end{aligned} \tag{9}$$

where $(x_\pm, y_\pm)$ are the locations of the peaks in the field. The chosen values are $\overline{x}_+ = \overline{x}_- = 0.5$, $\overline{y}_+ = 0.6$, $\overline{y}_- = 0.4$, and $\overline{\sigma} = 0.15$, where the bar indicates that these values are normalized in terms of $(N - 1)\Delta x$, the size of the grid. (All quantities in the code are non-dimensional, and where non-dimensional quantities are referred to in the text, a bar is used. Magnetic fields are normalized in terms of B_0, the peak field strength.)

3.1. Test case 1

First we consider a central current directed from the positive pole to the negative pole of the bipole. In particular we consider the choice

$$\overline{\alpha}_i = \begin{cases} C & \text{if } B_z(x_i, y_i, 0) > 0.95 B_0 \\ 0 & \text{otherwise,} \end{cases} \tag{10}$$

where C is a constant [note that $\overline{\alpha}_i$ is in units of the reciprocal of $(N-1)\Delta x$]. This configuration is similar to the 'uniform α' case considered by Sakurai (1981). In the following we consider the choices $C = 0.5, 1, 2, 3, 4, 8$.

Figure 1 illustrates the boundary conditions, for a grid with $N = 100$. The grey-scale background shows the distribution (9) of $B_z(x, y, 0)$, and the small crosses illustrate boundary points with $\overline{\alpha}_i = C$. There are 54 points with positive values of $\overline{\alpha}_i$, so there are 54 current-carrying field lines in the calculation.

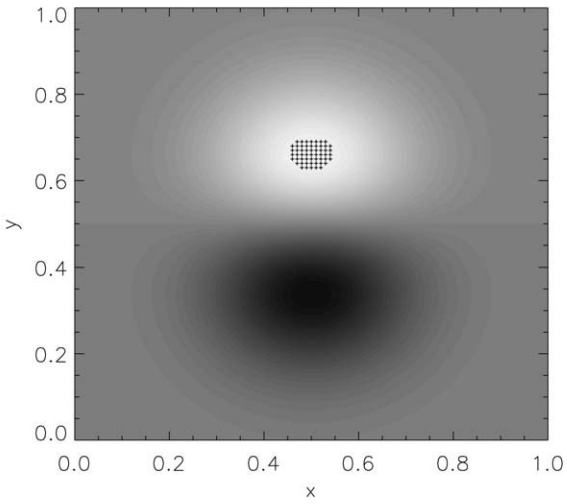

Figure 1. Boundary conditions for test case 1.

Figure 2 is a visualization of the potential field which is the starting point for each calculation. The view is from above the computational grid looking down, and the value of the field in the lower boundary is indicated by the greyscale. A number of field lines [starting from points with $B_z(x, y, 0) > 0.75B_0$] are shown for illustration.

For each choice of C, the code was run for a series of iterations, and the field configuration at each iteration was examined using visualizations such as Figure 2. The visualizations were used to judge whether the field had achieved an equilibrium configuration, where by 'equilibrium' we mean that field lines traced from given starting points (e.g., the field lines shown in Figure 2) do not appear to alter position between iterations. For $C = 0.5, 1, 2$ an equilibrium configuration was achieved at 10 iterations. For $C = 3$ an equilibrium was achieved at 30 iterations. For $C = 4$ the observed field lines were still oscillating slightly in position after 40 iterations, and for $C = 8$ no equilibrium was achieved in 50 iterations: the field was observed to alternate between a sequence of very different configurations.

Figure 3 shows the equilibrium configuration achieved for the case $C = 3$, which is the most non-potential case judged to have achieved an equilibrium. The view matches Figure 2. A transparent isocontour for current density defined by the set of points with $J > 0.25J_{\max}$ is shown, to indicate the region of high current. A twisted bipolar configuration is observed. This figure should be compared with Figure 3(b) in Sakurai (1981). Sakurai's figure suggests a weaker current than Figure 3, although it is hard to make a quantitative comparison based on the information in the paper. The appearance of Sakurai's Figure 3(b) is comparable with the results obtained with the present method for $C = 1$. The degree of non-potentiality

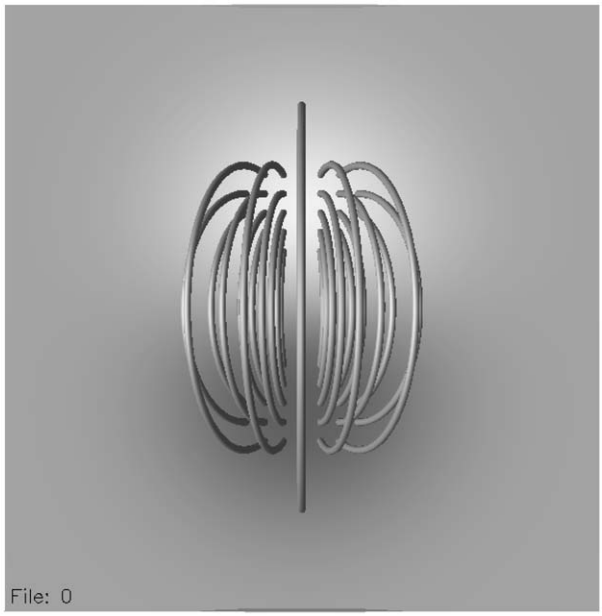

Figure 2. Initial potential field configuration.

in the present calculation may be estimated as follows. For a straight flux tube of length L a field line at radius r turns through an angle $\Delta\phi = B_\phi L/(B_z r)$ in traversing the tube. Taking $B_z = B_0$ and $B_\phi = \mu_0 I/(2\pi r)$ with $\mu_0 I \approx \alpha\pi r^2 B_0$ leads to $\Delta\phi = L\alpha/2$. For a flux loop we can take $L \approx \pi D/2$, where D is the distance between the footpoints of the loop. Hence we get $\Delta\phi = \pi\alpha D/4$. For the calculation with $C = 3$ we have $\overline{D} \approx 0.35$ and $\overline{\alpha} = 3$, leading to $\Delta\phi \approx 0.26\pi$. This estimate was checked by tracing field lines of the field in Figure 3. Specifically field lines originating at all boundary points $(x, y, 0)$ with $0.75B_0 < B_z(x, y, 0) < 0.95B_0$ were traced. The end point of each field line (the point where it returns to $z = 0$) was determined, and compared with the end point of the corresponding fieldline for the potential field. The angular displacement of the two end points (current-carrying and potential) about the minimum point of the boundary field was taken as the 'twist' of the field line. The average of the twist over the chosen set of field lines was found to be approximately 41 deg $\approx 0.23\pi$ rad.

Figure 4 gives a qualitative measure of how close to force-free the final configuration shown in Figure 3 is. In this figure four field lines originating near the peak of positive polarity in the boundary field are traced (dark tubes). The curl of the field (which is proportional to the current density) has been numerically evaluated, and the field lines of this field are also shown, for the same starting points (light tubes). For an exact force-free field the magnetic field lines and the 'current field lines'

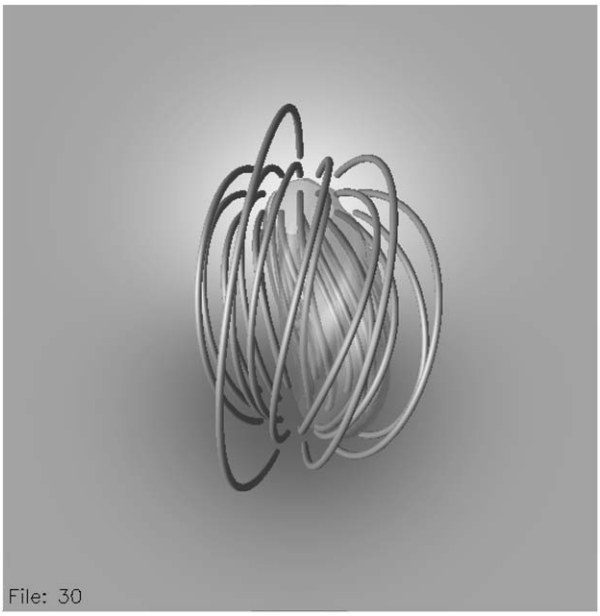

Figure 3. Visualization of field and current after 10 iterations for test case 1 with $C = 3$.

should coincide. The figure shows that the pairs of field lines slowly diverge from their common starting points. The observed error is likely due to several effects including the discretization of the current (the current and field of each current element are only exactly parallel on axis), truncation error in the calculation of the curl of the field, and errors due to interpolation of the field between gridpoints. Nevertheless the slow divergence of the current and magnetic field lines suggests that a fair approximation to a force-free field is being achieved.

A quantitative test of the success of the method was also applied. In the ideal force-free state the angle $\theta = \sin^{-1}[|\mathbf{J} \times \mathbf{B}|/(JB)]$ between the current density and the magnetic field is everywhere zero. However, for points with small values of J numerical estimates of this angle are not meaningful. Hence we consider the angle only for gridpoints close to the current-carrying field lines, i.e., with large values of J. In practice we calculate the average angle over points at which the magnitude of the curl of of the field is greater than one quarter of CB_0, which is a representative large value of $|\text{curl}\,\mathbf{B}|$.

Figure 5 shows the resulting average angles versus iteration, for the cases $C = 0.5$ (crosses), $C = 1$ (asterisks), $C = 2$ (diamonds) and $C = 3$ (triangles). The equilibrium achieved in each case is reflected in the average angle approaching a constant, at around 11, 9, 8, and 8 deg, respectively. We note that the angle is not expected to become zero, e.g., due to the discretization of the current. However,

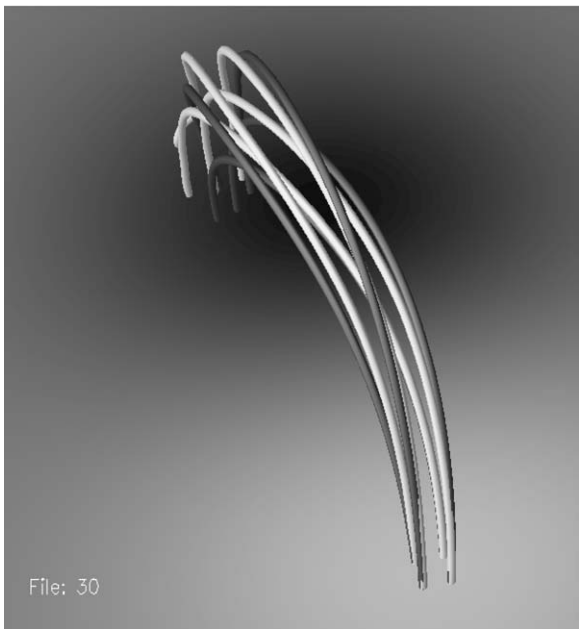

Figure 4. Field lines for the magnetic field and for the curl of that field near the centre of the bipole, for the configuration in Figure 3.

the observed values of the average angle suggest that a reasonable approximation to a force-free field is being achieved in each calculation.

Figure 6 shows the average angle versus iteration for the cases $C = 4$ (crosses) and $C = 8$ (asterisks), which did not achieve equilibria. For $C = 4$ the angle is still oscillating slightly after 40 iterations. For $C = 8$ the angle cycles through a sequence of values in subsequent iterations, and does not approach a constant value. This behavior is reminiscent of the bifurcation from a single fixed point to cycles observed in the iteration of simple one-dimensional nonlinear maps like the logistic equation (e.g., Thompson and Stewart, 2002).

The calculations presented above are for a grid with $N = 100$, but it is interesting to briefly consider results for other values of N. For example, for the cases which achieve equilibrium, the final value of the average angle between $\mathbf{J}$ and $\mathbf{B}$ is small but significant, and it is suggested that this is due to the finite grid. In that case the average angle should decrease with increasing N. To investigate this question, 20 iterations of the case $C = 3$ were calculated for $N = 50, 75, 100, 125, 150, 175$. Figure 7 shows the final value of the average angle versus N as a linear–log plot. The angle is observed to decrease slowly with increasing grid size, and a fit to a power law suggests an approximate $N^{-0.3}$ dependence. A second question is whether the equilibrium/non-equilibrium observed in Figures 5 and 6 depends on N. To address this question 20 iterations of the

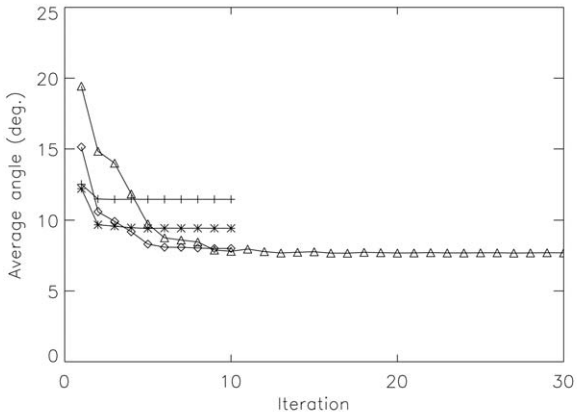

Figure 5. Mean angles between **J** and **B** versus iteration, for test case 1 with $C = 0.5$ (*crosses*), 1 (*asterisks*), 2 (*diamonds*) and 3 (*triangles*).

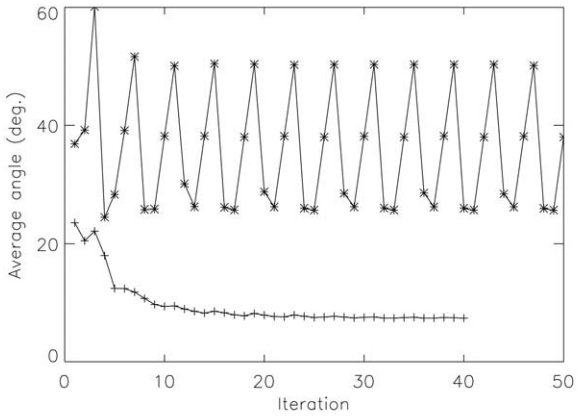

Figure 6. Mean angles between **J** and **B** versus iteration for test case 1 with $C = 4$ (*crosses*) and $C = 8$ (*asterisks*).

calculation with $C = 8$ were performed for $N = 50, 75, 100, 125, 150$. For each case oscillations similar to those shown in Figure 6 were observed, suggesting that the oscillatory behavior is independent of the size of the grid.

3.2. TEST CASE 2

As a second case we consider a central current which is directed from the positive pole to the negative pole for a number of points in the boundary for which $\overline{x} >$

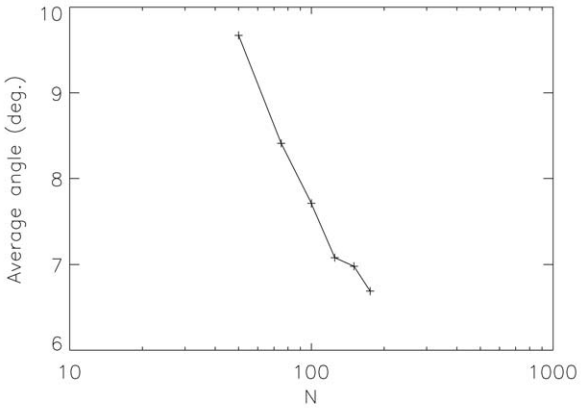

Figure 7. Mean angle between **J** and **B** after 20 iterations versus N for test case 1 with $C = 3$.

0.5, and is directed from the negative pole to the positive pole for a number of points in the boundary for which $\overline{x} < 0.5$, such that there is zero net axial current. Specifically we consider the choice

$$\overline{\alpha}_i = \begin{cases} C & \text{if } B_z(x_i, y_i, 0) > 0.95 B_0 \text{ and } \overline{x}_i > 0.5 \\ -C & \text{if } B_z(x_i, y_i, 0) > 0.95 B_0 \text{ and } \overline{x}_i < 0.5 \\ 0 & \text{otherwise,} \end{cases} \tag{11}$$

where C is a constant. This configuration is similar to the 'antisymmetric-α' case considered by Sakurai (1981). In the following we consider the cases $C = 0.5$, 1, 2, 4, 8, 16. Figure 8 illustrates the boundary conditions (cf., Figure 1). The small crosses (diamonds) indicate points with positive (negative) values of α_i. Once again there are 54 current-carrying field lines.

For $C = 0.5, 1, 2, 4$ equilibrium was achieved after 10 iterations, and for $C = 8$ a total of 30 iterations were required. For $C = 16$ the field configuration did not reach an equilibrium after 50 iterations. Figure 9 shows the equilibrium configuration for $C = 8$, the most non-potential case to achieve an equilibrium. A transparent isocontour is shown for points with $J > 0.25 J_{\max}$. In this case the configuration is symmetric in the plane $\overline{x} = 0.5$, and the non-potentiality shows up in the distorted shape of the field lines. Hudson and Wheatland (1999) argued that nonlinear force-free fields with symmetric boundary conditions in B_z but with antisymmetric currents should be symmetric, and this calculation supports the argument. This figure should be compared with Figure 4(a) in Sakurai (1981). Once again, the present calculation appears to be more highly non-potential.

Figure 10 shows the average angle between **J** and **B** (as defined in Section 3.1) versus iteration, for the cases $C = 0.5$ (vertical crosses), $C = 1$ (asterisks), $C = 2$ (diamonds), $C = 4$ (triangles), $C = 8$ (squares), and $C = 16$ (angled crosses). For $C = 0.5, 1, 2, 4, 8$ (cases where equilibrium was achieved) the average angle

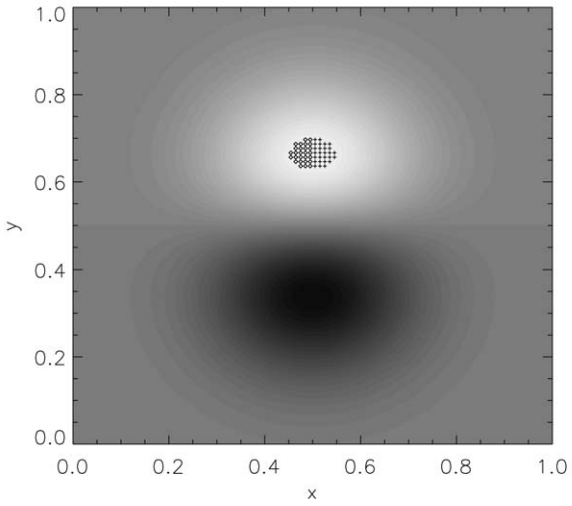

Figure 8. Boundary conditions for test case 2.

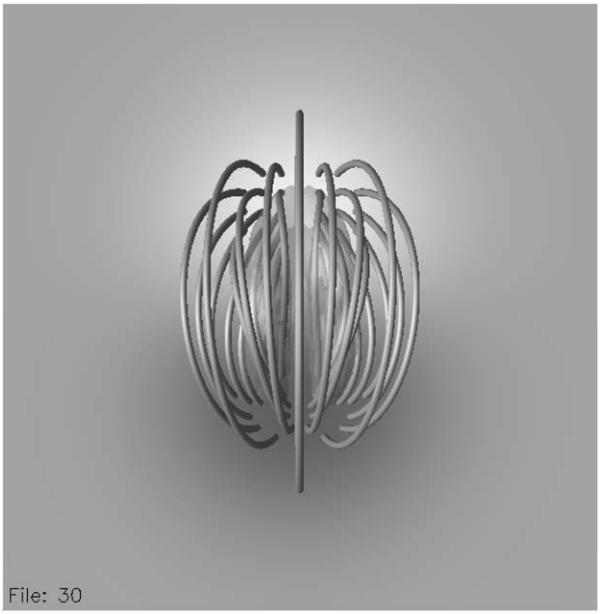

Figure 9. Visualization of field and current after 30 iterations for test case 2 with $C = 8$.

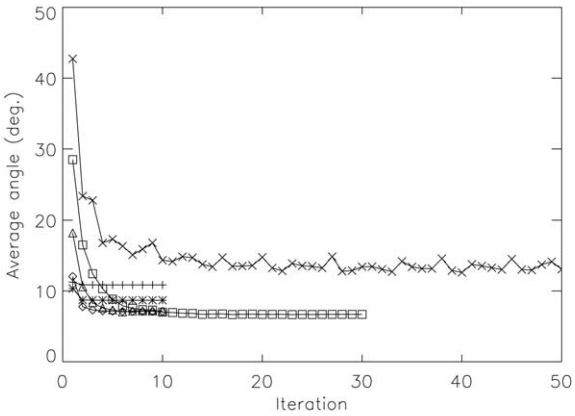

Figure 10. Mean angles between **J** and **B** versus iteration, for test case 2 with $C = 0.5$ (*crosses*), 1 (*asterisks*), 2 (*diamonds*), 4 (*triangles*), 8 (*squares*), and 16 (*angled crosses*).

approaches around 11, 9, 7, 7, and 7 deg, respectively. These results suggest that a fair approximation to a force-free field is being achieved. For $C = 16$ the angle decreases to around 13 deg but is still changing after 50 iterations.

Finally we consider the free energies of the calculated fields, for test cases 1 and 2, where by 'free energy' we mean the energy of the field minus the energy of the initial potential field. Figure 11 shows the results for test cases 1 (diamonds) and 2 (triangles), as log-log plots of free energy versus the value of C. For test case 1 the energies increase almost quadratically with C (exact quadratic dependence is indicated by the dashed line), which is expected on the basis of simple circuit models (e.g., Wheatland and Farvis, 2004). Specifically, the free energy of the field may be written as $E = \frac{1}{2}\sum_i L_i I_i^2 + \sum_{i>j} M_{ij} I_i I_j$, where I_i denotes the current on the ith current carrying field line, and L_i and M_{ij} are self and mutual inductances for the current circuits defined by the current-carrying field lines. We have $I_i \sim C$, and if the geometry of the field lines does not vary with the current then L_i and M_{ij} are constant, leading to $E \sim C^2$. However, for highly non-potential situations we expect the geometry of the circuits to depend on the current (Wheatland and Farvis, 2004), and hence the inductances will depend on the current. In this case quadratic dependence on C is no longer expected, and this may account for the results for test case 1 in Figure 11. Similar results are obtained for test case 2. The energies for case 2 are less than those for case 1, which is expected because the mutual inductance of oppositely directed current circuits is negative. The departure from $E \sim C^2$ behavior is again observed for large values of C, which may be attributed to dependence of the geometry of the current on the current.

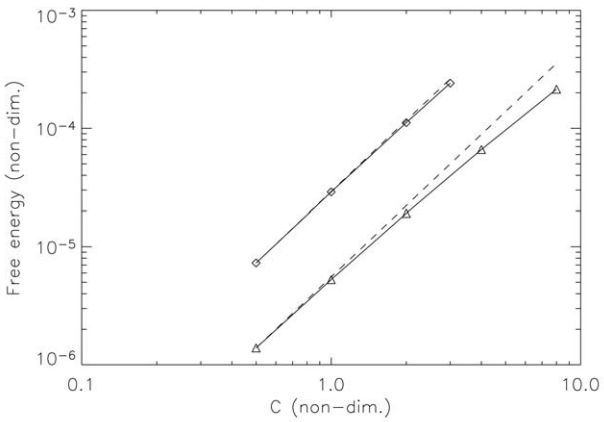

Figure 11. Free energies of fields for test cases 1 and 2.

4. Discussion and Conclusions

A method for calculating nonlinear force-free fields using current-field iteration and the Biot–Savart law is presented. The method is initially similar to Sakurai (1981) but differs in the way the problem is solved. In Sakurai's method a system of nonlinear equations is solved to determine the nodal points for a set of current-carrying field lines. In the present method the field at each gridpoint is directly calculated, based on a set of current-carrying field lines traced using the previous iteration of the field. An important feature of this approach is that it is straightforward to parallelize, because field contributions due to different current-carrying field lines add independently.

In this paper two test cases are considered, consisting of a bipolar magnetic configuration with symmetric and antisymmetric boundary distributions of current. The results of computations ranging from weakly non-potential to moderately non-potential are considered in each case. The method produces equilibrium configurations which are fair approximations to a force-free field for moderate numbers of iterations, including when there are substantial currents. For the most non-potential situations considered, equilibrium is not achieved. It is unclear whether this is due to the non-existence of a force-free equilibrium in these cases, or to a failure of the method. For the symmetric boundary conditions, the most non-potential case for which an equilibrium was found corresponds to a twist of around 0.25π. Other authors have reported force-free equilibrium configurations for bipoles carrying larger currents. For example, Klimchuk, Antiochos, and Norton (2000) used the magnetofrictional method to produce a configuration with a twist of 2π, although the boundary conditions were somewhat different to the present case. It is difficult to be definite on this point, given the absence of rigorous proofs of existence of solutions to the problem at hand.

The equilibrium configurations produced here are found to be reasonable approximations to a force-free state, judged by the average of the angle between the current density and magnetic field over points with large current density. The average is around seven degrees in the most non-potential cases. This result is for a grid size $N = 100$, and the angle is shown to decrease slowly with increasing grid size. It is argued that the finite value of the angle is due to discretization, although we have not been able to find a simple analytic argument to account for the size of the angle, or for the scaling of the angle with the number of grid points.

A point not discussed previously is the choice of a fixed value of α_i for a given footpoint at each iteration. The method of Sakurai (1981) also uses fixed values of α. In the general current-field iteration scheme described by Equation (4) the function α^k at iteration $k + 1$ can presumably be chosen in any way provided that the boundary values approach the required values for large k. McClymont, Jiao, and Mikić (1997) suggest that currents should be increased gradually. The effect of increasing α_i at each iteration to approach the value required by the boundary conditions will be investigated in future work.

In common with Sakurai's method, the present method is limited by the number of current-carrying field lines involved. In Sakurai's implementation this limitation was particularly restrictive, since the number of nonlinear simultaneous equations to be solved is twice the number of nodal points along current-carrying field lines. As a result the calculations in Sakurai (1981) involve only a small number of current-carrying field lines. In the present method this limitation is somewhat less restrictive because: (1) the method of solution is one of construction, and does not involve the solution of a large system of equations; and (2) the field line calculations are performed in parallel. The calculations presented here involve a moderate number of current-carrying field lines (54).

To pursue this point further, it is worthwhile to estimate the order of the two methods (i.e., to estimate how the number of calculations involved in the problem scales with the size N of the grid, in each case). In Sakurai's method, the number of current-carrying field lines may be taken to be fN^2, where f is the fraction of boundary points with a non-zero value of α_i. Each current-carrying field line will have of order N nodal points, leading to a total $\sim fN^3$ nodal points. The method then involves solving a system of $\sim fN^3$ simultaneous equations, which is a problem of order $(fN^3)^3 = f^3N^9$ (Press *et al.*, 1992). For comparison, consider the present method. Once again each current-carrying field line has of order N nodal points. The field at N^3 points in the box needs to be calculated based on each nodal point, so there are $\sim N \times N^3 = N^4$ calculations involved in this procedure. Once again if we assume fN^2 current-carrying field lines, then a serial version of the method is of order fN^6. The parallel version of the code should be considerably faster. As an idealization (ignoring overheads involved in parallelization) if there are M processes, then the method is of order fN^6/M. This suggests that, for large N, a small fraction f and/or large scale parallelization is required.

The code used here is a parallel implementation of the method using OpenMP (Chandra *et al.*, 2001), which was run on an eight-processor shared memory machine. A code using the Message Parsing Interface (MPI; see, e.g., Gropp, Lusk, and Skjellum, 1999), suitable for distributed memory computers, has also been written and tested. The MPI version of the code will be used on a cluster to enable calculations with substantially larger numbers of current-carrying field lines. This is likely to be necessary, e.g., to apply the code to vector magnetograms.

There are many potential applications of the present method for calculating force-free fields in solar physics (e.g., see the discussion in McClymont, Jiao, and Mikić, 1997). A longer-term goal is to develop the code described here into a robust tool for use by the wider solar physics community, to assist in the analysis of data from the next generation of vector magnetographs.

Acknowledgements

M.S.W. acknowledges helpful discussions with Dave Galloway, and the support of an Australian Research Council QEII Fellowship.

References

Alissandrakis, C. E.: 1981, *Astron. Astrophys.* **100**, 197.
Amari, T., Boulmezaoud, T. Z., and Mikić, Z.: 1999, *Astron. Astrophys.* **350**, 1051.
Amari, T., Aly, J. J., Luciani, J. F., Boulmezaoud, T. Z., and Mikić, Z.: 1997, *Solar Phys.* **174**, 129.
Bineau, M.: 1972, *Commun. Pure Appl. Math.* **25**, 77.
Chandra, R., Dagum, Kohr, D., Maydan, D., McDonald, J., and Menon, R.: 2001, *Parallel Programming in OpenMP*, Morgan Kaufmann, San Francisco.
Grad, H. and Rubin, H.: 1958, in *Proc. 2nd Int. Conf. on Peaceful Uses of Atomic Energy*, Vol. 31, United Nations, Geneva, p. 190.
Gropp, W., Lusk, E., and Skjellum, A.: 1999, *Using MPI: Portable Parallel Programming with the Message-Passing Interface*, 2nd ed., MIT Press, Cambridge, Massachusetts.
Hudson, T. S. and Wheatland, M. S.: 1999, *Solar Phys.* **186**, 301.
Keller, C. U., Harvey, J. W., and Giampapa, M. S.: 2003, in S. L. Keil and S. V. Avakyan (eds.), *Innovative Telescopes and Instrumentation for Solar Astrophysics*, Proceedings of the SPIE, Vol. 4853, p. 194.
Klimchuk, J. A., Antiochos, S. K., and Norton, D.: 2000, *Astrophys. J.* **542**, 504.
Li, J.-Q., Wang, J.-X., and Wei, F.-S.: 2003, *Chin. J. Astrophys.* **3**, 247.
Lin, H., Penn, M. J., and Tomczyk, S.: 2000, *Astrophys. J.* **541**, L83.
Marsh, G. E.: 1996, *Force-free Magnetic Fields: Solutions, Topology and Applications*, World Scientific, Singapore.
McClymont, A. N., Jiao, L., and Mikić, Z.: 1997, *Solar Phys.* **174**, 191.
Press, W. H., Teukolsky, S. A., Vetterling, W. T., and Flannery, B. P.: 1992, *Numerical Recipes in C: The Art of Scientific Computing*, 2nd ed., Cambridge University Press, Cambridge.
Priest, E. R. and Forbes, T. G.: 2002, *Astron. Astrophys. Rev.* **10**, 313.
Régnier, S., Amari, T., and Kersalé, E.: 2002, *Astron. Astrophys.* **392**, 1119.
Sakurai, T.: 1981, *Solar Phys.* **69**, 343.

Sakurai, T.: 1989, *Space Sci. Rev.* **51**, 11.
Thompson, J. M. T. and Stewart, H. B.: 2002, *Nonlinear Dynamics and Chaos*, Wiley, Chichester.
Wheatland, M. S.: 2004, in T. Sakurai and T. Sekii (eds.), *The Solar-B Mission and the Forefront of Solar Physics', Proceedings of the Fifth Solar-B Meeting held in Roppongi*, Japan, *ASP Conference Series*, in press.
Wheatland, M. S. and Farvis, F. J.: 2004, *Solar Phys.* **219**, 109.
Wheatland, M. S., Sturrock, P. A., and Roumeliotis, G.: 2000, *Astrophys. J.* **540**, 1150.
Wiegelmann, T. and Inhester, B.: 2003, *Solar Phys.* **214**, 287.
Yan, Y. and Sakurai, T.: 2000, *Solar Phys.* **195**, 89.